Nuclear Astrophysics in the Storage Ring: Background Suppressed Simultaneous Measurement of (p,γ) and (p,n) Reactions

L. Varga,[1,2,3,4,*] J. Glorius,[1,†] M. Aliotta[2,5] K. Blaum[6] L. Bott,[7] C. Brandau,[1,8] B. Brückner,[7] C. G. Bruno[2]
X. Chen[9] R. Chen,[1,9] S. Dababneh,[10] T. Davinson[2] D. Dmytriiev,[1] S. F. Dellmann[7,29] I. Dillmann,[11,12] P. Erbacher[7]
S. Fiebiger[7] O. Forstner,[1,13] T. Gaßner,[1] K. Göbel[1] S. Goriely,[14] C. J. Griffin[11] R. E. Grisenti,[1,7] M. Groothuis,[7]
A. Gumberidze[1] G. Gyürky,[15] M. Heil[1] R. Hensch,[7] R. Hess[1] P.-M. Hillenbrand,[1,8] P. Hillmann,[7] O. Hinrichs,[7]
R. Joseph[1] B. Jurado[16] T. Kausch,[7] K. Khasawneh,[7] A. Khodaparast,[1,7] T. Kisselbach[7] N. Klapper,[7]
C. Kozhuharov[1] D. Kurtulgil,[7] G. J. Lane[17] C. Langer,[7,18] G. Leckenby[11,19] C. Lederer-Woods,[2] M. Lestinsky[1]
Yu. A. Litvinov[1] S. Litvinov,[1] B. Löher[1] E. Lorenz,[7] B. Lorentz,[1] P. Marini[16] J. Marsh[2] E. Menz[1]
T. Morgenroth,[1] T. T. Nguyen,[7] F. Nolden,[1] N. Petridis[1] U. Popp,[1] A. Psaltis,[20] M. Reed[17] R. Reifarth,[7,29]
M. S. Sanjari[1,18] D. Savran[1] M. Sguazzin,[16] H. Simon[1] R. S. Sidhu[2,26] Z. Slavkovská,[7,17] U. Spillmann[1]
M. Steck,[1] T. Stöhlker,[1,13,27] J. Stumm,[7] A. Surzhykov,[21,22] J. Swartz[16] T. Szücs,[15] A. Taremi Zadeh,[7] B. Thomas[7]
S. Yu. Torilov[23] H. Törnqvist[1,20] M. Träger,[1] C. Trageser,[1,8] S. Trotsenko,[1] D. Vescovi[7,28] M. Volknandt,[7]
H. Weick[1] M. Weigand,[7] C. Wolf,[7] P. J. Woods,[2] Y. M. Xing[9,1] and T. Yamaguchi[24,25]

[1]*GSI Helmholtzzentrum für Schwerionenforschung GmbH*, Darmstadt, Germany
[2]*University of Edinburgh*, Edinburgh, United Kingdom
[3]*Technische Universität München*, Garching b. München, Germany
[4]*Excellence Cluster ORIGINS*, Garching, Germany
[5]*ExtreMe Matter Institute EMMI, GSI Helmholtzzentrum für Schwerionenforschung GmbH*, Darmstadt, Germany
[6]*Max-Planck-Institut für Kernphysik (MPIK)*, Heidelberg, Germany
[7]*Goethe Universität, Frankfurt* am Main, Germany
[8]*Justus-Liebig Universität, Gießen*, Germany
[9]*Institute of Modern Physics*, Chinese Academy of Sciences, Lanzhou, China
[10]*Al-Balqa Applied University*, Salt, Jordan
[11]*TRIUMF*, Vancouver, British Columbia, Canada
[12]*Department of Physics and Astronomy, University of Victoria*, Victoria, British Columbia, Canada
[13]*Helmholtz-Institut Jena*, Jena, Germany
[14]*Institut d'Astronomie et d'Astrophysique, Université Libre de Bruxelles*, Brussels, Belgium
[15]*HUN-REN Institute for Nuclear Research*, Debrecen, Hungary
[16]*Université de Bordeaux, CNRS, LP2I Bordeaux*, Gradignan, France
[17]*Australian National University*, Canberra, Australian Capital Territory, Australia
[18]*FH Aachen University of Applied Sciences*, Jülich, Germany
[19]*Department of Physics and Astronomy, University of British Columbia*, Vancouver, Canada
[20]*Technische Universität Darmstadt*, Darmstadt, Germany
[21]*Physikalisch-Technische Bundesanstalt*, Braunschweig, Germany
[22]*Technische Universität Braunschweig*, Braunschweig, Germany
[23]*St. Petersburg State University*, St. Petersburg, Russia
[24]*Department of Physics, Saitama University*, Saitama, Japan
[25]*Tomonaga Center for the History of the Universe, University of Tsukuba*, Ibaraki, Japan
[26]*University of Surrey*, Guildford, United Kingdom
[27]*Institut für Optik und Quantenelektronik, Friedrich-Schiller-Universität Jena*, Jena, Germany
[28]*Istituto Nazionale di Astrofisica, Osservatorio Astronomico d'Abruzzo*, Teramo, Italy
[29]*Los Alamos National Laboratoy*, Los Alamos, USA

We report the application of the new elimination of Rutherford elastic scattering technique for the measurement of proton-induced reaction cross sections utilizing stored ions decelerated to astrophysical energies. This approach results in a background reduction factor of about 1 order of magnitude, enabling

*Contact author: l.varga@gsi.de
†Contact author: j.glorius@gsi.de

the first measurement of a (p, n) cross section in a storage ring. Here, the reaction channels $^{124}\text{Xe}(p, n)$ and $^{124}\text{Xe}(p, \gamma)$ have been studied just above the neutron threshold energy. The new data provide valuable constraints for Hauser-Feshbach theory and extrapolation of the (p, γ) cross section to lower energies. Most importantly, for nuclei of limited availability, the method represents a powerful improvement to efficiently study proton-induced reactions at energies within or close to the astrophysical Gamow window, bringing many reaction measurements within reach that were previously inaccessible in the laboratory.

The nuclear physics of stars governs stellar evolution and nucleosynthesis and thereby facilitates the diverse story of cosmic element genesis. Today, after nearly a century of active research in nuclear astrophysics, a rich and complex picture has emerged [1]. It is, however, far from being complete. One of the long-standing issues is the origin of the p nuclei, around 35 neutron-deficient, stable isotopes between ^{74}Se and ^{196}Hg that are bypassed by neutron-capture nucleosynthesis otherwise predominant for the creation of elements heavier than Fe. According to astrophysical simulations, the so-called γ process in different types of supernovae is able to produce the bulk of the p nuclei, but a variety of further explosive processes, such as the νp or rp processes, potentially contribute in the lower mass region [2–5]. The large nuclear reaction networks arising under such extreme conditions act predominantly in the realm of unstable nuclei, where nuclear cross sections and stellar reaction rates, one of the main ingredients of nucleosynthesis models, are entirely based on nuclear theory. Measured cross sections of photodissociation, radiative capture, or charge-exchange reactions, i.e., $(p, \gamma) \leftrightarrow (\gamma, p)$ and $(p, n) \leftrightarrow (n, p)$, are needed to reduce the large and mostly unknown uncertainties of nuclear theory in this domain.

The requirements for such experiments are very high and the most promising approach is to employ rare ion beam (RIB) technologies. However, due to the small reaction cross sections that are usually involved at the low energies of interest in nuclear astrophysics, as well as the available RIB intensity and purity in the heavier mass regions, only a single successful RIB measurement of relevance for the p nuclei has been accomplished so far [6]. One way to overcome these limitations is to utilize a heavy-ion storage ring as it has been demonstrated in studies of $^{96}\text{Ru}(p, \gamma)$ [7] and $^{124}\text{Xe}(p, \gamma)$ [8] reactions at the experimental storage ring (ESR) at GSI [9,10].

In this Letter, we focus on the report of the elimination of Rutherford elastic scattering (ERASE) technique in heavy-ion storage rings. Its application increases the signal-to-background ratio for direct proton-induced reaction cross section measurements by about an order of magnitude. The strength and validity of the new method is demonstrated on the cases of $^{124}\text{Xe}(p, \gamma)$ and $^{124}\text{Xe}(p, n)$ measured simultaneously at center-of-mass (c.m.) energies just above the

(p, n) reaction threshold. The new approach facilitates future studies of proton-capture or charge-exchange reactions on rare, low-energy ion beams, which are pivotal to our understanding of explosive nucleosynthesis and nuclear structure [11–13].

The ESR enables accumulation, storage, cooling, and deceleration of heavy-ion beams as well as additional means of purification for exotic beams after in-flight production in the fragment separator [14–16]. The basic layout of the proton-capture campaign shall be summarized here briefly: bare and potentially exotic ions, produced at energies above 100 MeV/u are injected and accumulated in the ESR [17]. When the stored ions are subsequently decelerated to energies of astrophysical relevance, they orbit in the ring at frequencies of a few 100 kHz. As a result, the luminosity for reaction studies with the internal gas target is boosted by about 5 orders of magnitude compared to single-pass experiments [8]. For proton-induced reactions, a thin, ultrapure hydrogen gas jet of about 10^{14} atoms/cm^2 is available [18], which enables an energy resolution on the order of 20 keV. The detection scheme is based on interception of the heavy reaction recoils after separation from the stored beam in the field of the dipole magnet downstream of the internal target. For the purpose of normalization, the entire measurement is done relative to the radiative capture of an electron from the hydrogen into the atomic K shell of the bare projectile ion, the so-called K-REC process [19].

The detector position in the dipole magnet is equipped with a $W1$-type double-sided silicon strip detector (DSSD) by Micron Semiconductors, Ltd. [20]. To enable detection of the low-energy recoil ions, it is situated directly inside the vacuum chamber and meets the requirements of the ultrahigh vacuum environment of the ring. The ^{125}Cs recoils from the (p, γ) reaction form a narrow kinematic cone, due to the negligible momentum carried by the γ rays and can be detected with an efficiency of $\epsilon = 100\%$. For the (p, n) reaction channel, which opens for $E_{\text{c.m.}} > |Q_{(p,n)}| = 6.73$ MeV, the emitted neutron carries more momentum and causes a larger recoil cone, which partly extends beyond the active area of the detector, especially for energies $E_{\text{c.m.}} \gtrsim 7.7$ MeV. This allows detection efficiencies in the range of $\epsilon = 70\%$–100%. However, both signatures are fully or partially overlayed by a strong
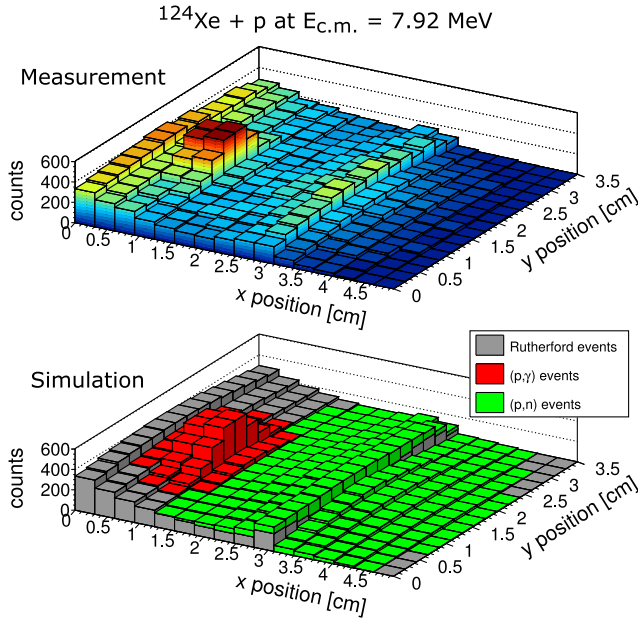
FIG. 1. Upper: A DSSD spectrum measured at $E_{c.m.} = 7.92$ MeV is shown. Lower: Monte Carlo simulation of the experimental spectrum. It is constructed by fitting three individual components: Rutherford scattering of ^{124}Xe ions off the H target (gray), and the (p,γ) and (p,n) recoil distributions (red and green, respectively).

background distribution from Rutherford (RF) elastic scattering [21], as shown in Fig. 1. While it has been demonstrated that a pure RF model for the background can be used in the present energy range to deduce an absolute in-ring luminosity [22], it limits the overall sensitivity of the method.

All the (re)analyzed data here are above the (p,n) threshold between 6.96 and 10.06 MeV in c.m. energies and have either been taken from [8] or from the new experiment. See labeling in Table I for details.

The ion hit distribution on the DSSD at $E_{c.m.} = 7.92$ MeV is shown in the upper panel of Fig. 1. The radial and vertical directions with respect to the storage ring geometry are labeled as x and y, pointing inward and up, respectively. The lower panel of Fig. 1 demonstrates how well the experimental spectrum is reproduced by fitting a composition of Monte Carlo simulations for each component based on the MOCADI code [24]. While the (p,γ) cluster (red) sits on the tail of the RF distribution (gray), the center of the (p,n) distribution (green) is located on its edge.

The simulation of the RF component is performed using an estimated emittance for the stored beam [25], the realistic beam optics of the ESR, and the two-body kinematics, as well as the angular distribution of the scattering process. The simulation of the nuclear reaction distributions is more complex. It involves modeling the decay behavior of the compound nucleus including the γ cascade for (p,γ) and, additionally, the populated state in ^{124}Cs after neutron-emission in case of the (p,n) reaction.

TABLE I. Cross sections of ^{124}Xe(p,γ) and ^{124}Xe(p,n). Values of intermediate analysis steps are given in Supplemental Material [23]. The energy uncertainty for all data points is about 20 keV.

Reaction	$E_{c.m.}$ (MeV)	$\sigma_{(p,x)}$ (mb)
^{124}Xe(p,γ)[a]	6.96	$103.6 \pm 2.0_{stat} \pm 5.8_{sys}$
^{124}Xe(p,γ)		$70.7 \pm 3.4_{stat} \pm 5.6_{sys}$
^{124}Xe(p,γ)[b]	7.05	$69.8 \pm 2.2_{stat} \pm 4.9_{sys}$
^{124}Xe(p,n)[b]		$25.0 \pm 1.5_{stat} \pm 1.8_{sys}$
^{124}Xe(p,γ)[a]	7.92	$43.4 \pm 1.6_{stat} \pm 2.6_{sys}$
^{124}Xe(p,n)		$192.8 \pm 2.7_{stat} \pm 14.5_{sys}$
^{124}Xe(p,γ)[b]	10.06	$23.9 \pm 3.4_{stat} \pm 5.0_{sys}$
^{124}Xe(p,n)[b]		$437.8 \pm 11.2_{stat} \pm 50.1_{sys}$

[a]Reanalyses from [8].
[b]Measurements with application of the new ERASE technique.

In practice, however, the (p,γ) recoil cluster can be well approximated by a 2D Gaussian distribution, because a multistep γ cascade is present, resulting in a blur that dominates the shape of the distribution.

In order to disentangle the two extended distributions of RF and (p,n), two approaches are compared here. First, we introduce a model based on the energy-binned population of ^{124}Cs after neutron emission, called the "SIM model" in the following. For each bin between $E_{c.m.} + Q$ and the ground state of ^{124}Cs, the two-body kinematics, the subsequent γ cascade, and the ion optical system in the ESR are simulated individually. The closer the populated bin is to the ground state (and the higher the energy of the emitted neutron n_i), the larger the recoil cone. This results in a superposition of N distributions of different sizes, which is then used to fit the measured dataset, featuring a free scaling parameter for each (p,n_i) component. The other approach assumes a simple Gaussian shape also for the (p,n) distribution and is referred to as the "GAUSS model" below. Both fits reproduce the data within statistical error bars, see Fig. 2, but due to the reduced parameter space, the GAUSS model has less critical convergence criteria.

To determine the number of measured (p,γ) or (p,n) events, the kinematically allowed area of the distribution of interest is integrated and the other two fit components are considered as background and subtracted. The number of counts extracted this way depends only weakly on the (p,n) fit model, showing variations of 2% and 0.5% for (p,γ) and (p,n), respectively. In cases where the detection efficiency for the (p,n) recoils is not 100%, i.e., at $E_{c.m.} = 7.92$ and 10.06 MeV, it needs to be calculated based on the fit. For the dataset of ^{124}Xe(p,n) at $E_{c.m.} = 7.92$ MeV, this efficiency shows variations of 2.5% between the GAUSS and the SIM models.

To enable the analysis of the low-statistics measurements at $E_{c.m.} = 10.06$ MeV, the GAUSS model is used consistently for all data points. The statistical error accounts for
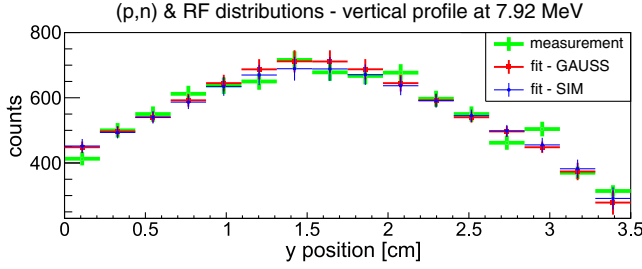
FIG. 2. The projection of ion hits in x strips 9–11 onto the y axis representing a vertical profile of the (p, n) + RF distributions at 7.92 MeV. The measurement (green) is compared to the fits based on the SIM (blue) and GAUSS (red) models. Both models reasonably agree with the measurement.
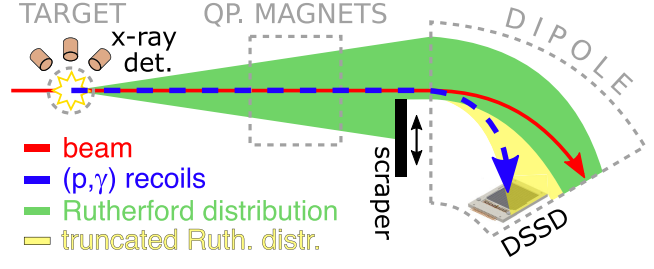

FIG. 3. The relevant section of the ESR is shown schematically with the placement of the scraper device and the detectors. Additionally, the principle of the ERASE background suppression technique is sketched. See text for details.

the measurement uncertainty before the background subtraction, as follows conveniently from Poisson statistics. The systematic uncertainties have several components. For the (p, γ) distribution, the leading term originates from the fit, which is $\gtrsim 5\%$, including the model variations mentioned above. For the (p, n) distribution, the two major contributions to the systematic error are the uncertainty of the fit itself ($\gtrsim 5\%$) and the calculation of the detection efficiency in the relevant cases (2.5%). Additionally, the cross section normalization contributes to the systematic uncertainties in all cases (2%) [26].

Based on a relative measurement to the K-REC cross section using x-ray spectroscopy at the gas target, as described in [8], the number of (p,x) events is converted into a cross section. The cross section values and related uncertainties are given in Table I. The reexamined (p, γ) cross sections at 6.96 and 7.92 MeV are in good agreement with the results from [8], see also Fig. 5.

As demonstrated in [8], the signal-to-background ratio (SBR) for (p, γ) measurements diminishes toward lower energies, increasing the uncertainty of the measured cross sections. This is caused by the divergent behavior of the (p, γ) and RF cross sections and severely limits the sensitivity of the method. In addition, the uncertainties are expected to grow for low beam intensity scenarios such as measurements involving RIBs. Hence, it is crucial for future measurements to improve the sensitivity for proton-capture detection. One way to do so is to reduce the background by discriminating or blocking the Rutherford scattering events on the particle detector. For this purpose, the ERASE technique has been developed.

Ion optical simulations using the MOCADI code [24] showed that such a blocking can be achieved in the ESR. Figure 3 illustrates the concept of ERASE. To reduce additional scattering off the edge, following [27], a scraper with a highly polished double-edge surface was installed on a pneumatic piston. It was placed 6 m downstream of the gas target just in front of the dipole magnet and could be rapidly positioned with submillimeter precision, enabling precise trimming of the local ring acceptance. However, the

initial beam preparation in the ESR, mainly during injection and deceleration, requires large acceptance to avoid beam losses, which demands an automatic movement of the device at the start and the end of the measurement phase. With this technique the extended RF cone can be partially blocked on the inner ring trajectories while leaving the reaction products of (p, γ) and (p, n) unaffected, which remain centered on the storage orbit before entering the dipole field. This effectively blocks the scattering distribution that emerges under c.m. angles in the range between 40° and 140°, which is the dominant part of the RF background for the (p, γ) and (p, n) signatures. However, due to its lower momentum, the RF backscattering component to larger angles is still partly deflected onto the detector, resulting in a weak residual background. The technique has been verified through a measurement of $^{124}\text{Xe}(p, \gamma)$ reaction at $E_{\text{c.m.}} = 7.05$ MeV. The scraping edge was either not in use or positioned 25.0 ± 0.5 mm away from the stored beam. The obtained cross sections are in excellent agreement, as shown in Table I, where ERASE measurements are marked with a "b."

Figure 4 shows the DSSD hit map without ERASE technique in the upper panel and with ERASE in the lower panel. At this c.m. energy the (p, n) channel is only ≈ 300 keV above threshold, which leads to a narrow recoil cone and a signature similar to the (p, γ) reaction but weaker in intensity. With the previous technique, the (p, γ) cluster at $x = 2.76 \pm 0.01$ cm sits on the tail of an intense RF background, which completely conceals the (p, n) signature. When the scraper is in position, though, the RF background is dramatically reduced, facilitating identification and analysis of the (p, n) channel even in this situation. Note that the DSSD was moved by about 6 mm away from the beam for the ERASE dataset to enable full coverage for (p, n) detection.

The improvement of the sensitivity for the case of the (p, γ) analysis can be quantified by comparing the SBR for both settings, i.e., the number of (p, γ) events after background subtraction divided by the number of relevant background counts. The ratio R of SBRs for the ERASE and original setting was measured as $R = 7.9 \pm 1.4$ at

FIG. 5. All data points of the ^{124}Xe + p reactions from this Letter and Glorius *et al.* [8]. Solid and dashed lines represent theoretical calculations for the (p, γ) and (p, n) reaction cross sections. For more details, see text.
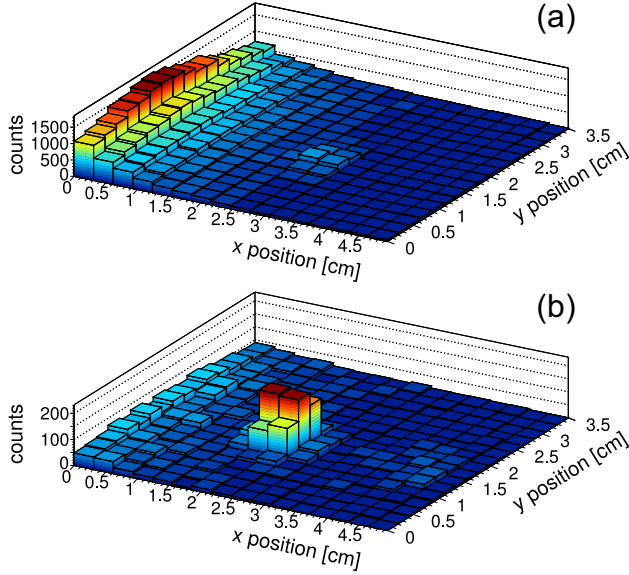
FIG. 4. The effect of the new background suppression technique is demonstrated by comparing the DSSD spectrum of the original setting (a) with the one of the ERASE setting (b) at 7.05 MeV. Apart from the scraper, only the position of the detector was changed by $\Delta x = 6$ mm between (a) and (b).

$E_{\text{c.m.}} = 7.05$ MeV, indicating a clear sensitivity boost. Further, the validity of the updated technique is demonstrated by the excellent agreement of the cross section results for both settings at this energy.

Caused by secondary scattering on the scraper, the measured ERASE spectrum shows a smooth decline rather than a sharp cutoff of the RF distribution at $x = 0$–1.5 cm. While it partly reaches the (p, γ) signature, its contribution is negligible in comparison to the number of (p, γ) events in this case. For the analysis, the truncated RF background was taken into account as a 2D polynomial fit.

It should be noted that in the present case the effect on the (p, γ) cross section uncertainty is not strong, as the high count rate in the (p, γ) channel alone allows a reliable analysis. In contrast, the (p, n) channel shows rather low statistics and a broad recoil distribution around 7 MeV. An extraction of the (p, n) cross section in this situation was only possible through the benefits of ERASE, i.e., at 7.05 MeV, but not at 6.96 MeV where ERASE was not available. This demonstrates how critical the new method will be when eventually dealing with rare ions of limited intensity and/or lower beam energies where low (p, γ) rates and increased RF rates will dominate the uncertainty.

In the following, the newly extended dataset for proton-induced reactions on ^{124}Xe is compared to theory calculations based on the Hauser-Feshbach formalism as implemented in the code TALYS1.96 [28]. Inside the Gamow energy window, the cross section predictions for radiative proton capture dominantly depend on the proton optical model potential (OMP). However, around and above the (p, n) channel
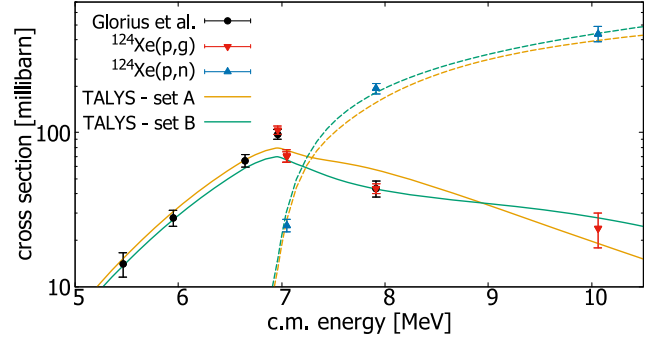
opening, the (p, γ) cross section becomes additionally sensitive to the photon-strength function (PSF) as well as the nuclear level density (NLD) [29]. This situation often complicates the extraction of direct constraints for the OMP from (p, γ) measurements in this energy range. Facilitated by the new (p, n) data points, we can now partly resolve this ambiguity, due to the fact that predictions for the (p, n) channel are again dominantly sensitive to the proton OMP. Hence, the additional (p, n) data allow for a more profound judgment of the OMP, which is central to extrapolations toward lower energies.

In Fig. 5 the measured data points are shown in comparison to statistical model predictions based on different models for the above mentioned input parameters. Here, we consider two sets (called *A* and *B*) of input parameters available in TALYS1.96, that are able to reproduce the full dataset with comparable quality. Both sets are based on the the the optical potential by Jeukenne *et al.* (JLM-B) [30] obtained with the Skyrme-Hartree-Fock-Bogoliubov (HFB) matter densities [31], which is the only OMP that reproduces the global energy dependence of (p, γ) below and (p, n) above the threshold. Further, set *A* consists of nuclear inputs consistently extracted from microscopic models, i.e., the temperature-dependent Gogny-HFB plus combinatorial NLD [32] and the Gogny-HFB plus Quasiparticle Random-Phase Approximation (QRPA) PSF for $E1$ and $M1$ channels [33]. In contrast, set *B* concerns ingredients derived within more phenomenological approaches, i.e., the constant-temperature plus Fermi gas NLD [34] and the simple modified Lorentzian model for the total dipole PSF [35,36].

Both sets result in an acceptable reproduction of the cross sections and show a very similar trend toward lower energies, thus both are suitable for extrapolation into the Gamow window. Set *B*, however, does perform slightly better above the (p, n) threshold for both reaction channels.

It should be noted that the enhancement of the (p, γ) cross section as measured in [8] at 6.96 MeV, cannot be described by any of our calculations that successfully

reproduce the full dataset. This might be connected to the neutron channel opening at 6.73 MeV and/or to the rather strong deformation predicted for ^{124}Xe [37], which is not explicitly accounted for in the OMP used here.

In conclusion, the new ERASE technique enables the first measurement of a (p, n) reaction cross section in the storage ring environment. This is facilitated by a signal-to-background ratio improved by about 1 order of magnitude, which also impacts the sensitivity of (p, γ) reaction studies established in the past. The new technique enabled the measurement of ^{124}Xe(p, n) and ^{124}Xe(p, γ) just above the reaction threshold and opens the door for future radioactive beam experiments at low energy and limited intensity. In case both (p, γ) and (p, n) channels are open, their simultaneous investigation will be routinely possible. Such combined measurements inside and above the astrophysical Gamow window, in general, provide critical constraints for cross section predictions highly relevant in the explosive nucleosynthesis of various stellar scenarios. The ability to precisely define the c.m. energy allows for fine searching of abrupt changes of cross section trends. The observed sudden drop of the ^{124}Xe(p, γ) cross section at the (p, n) threshold is confirmed by data from two independent measurements. Further research is needed to uncover the nature of this drop.

[1] M. Arnould and S. Goriely, Prog. Part. Nucl. Phys. **112**, 103766 (2020).

[2] M. Pignatari, K. Göbel, R. Reifarth, and C. Travaglio, Int. J. Mod. Phys. E **25**, 1630003 (2016).

[3] A. Choplin, S. Goriely, R. Hirschi, N. Tominaga, and G. Meynet, Astron. Astrophys. **661**, A86 (2022).

[4] C. Fröhlich, G. Martínez-Pinedo, M. Liebendörfer, F.-K. Thielemann, E. Bravo, W. R. Hix, K. Langanke, and N. T. Zinner, Phys. Rev. Lett. **96** (2006).

[5] H. Schatz and K. Rehm, Nucl. Phys. **A777**, 601 (2006).

[6] G. Lotay, S. A. Gillespie, M. Williams, T. Rauscher, M. Alcorta, A. M. Amthor, C. A. Andreoiu, D. Baal, G. C. Ball, S. S. Bhattacharjee *et al.*, Phys. Rev. Lett. **127**, 112701 (2021).

[7] B. Mei, T. Aumann, S. Bishop, K. Blaum, K. Boretzky, F. Bosch, C. Brandau, H. Braeuning, T. Davinson, I. Dillmann *et al.*, Phys. Rev. C **92**, 035803 (2015).

[8] J. Glorius, C. Langer, Z. Slavkovská, L. Bott, C. Brandau, B. Brueckner, K. Blaum, X. Chen, S. Dababneh, T. Davinson *et al.*, Phys. Rev. Lett. **122**, 092701 (2019).

[9] B. Franzke, Nucl. Instrum. Methods Phys. Res., Sect. B **24–25**, 18 (1987).

[10] GSI: GSI Helmholtzzentrum für Schwerionenforschung, http://www.gsi.de.

[11] T. Rauscher, N. Nishimura, R. Hirschi, G. Cescutti, A. S. J. Murphy, and A. Heger, Mon. Not. R. Astron. Soc. **463**, 4153 (2016).

[12] N. Nishimura, T. Rauscher, R. Hirschi, G. Cescutti, A. S. J. Murphy, and C. Fröhlich, Mon. Not. R. Astron. Soc. **489**, 1379 (2019).

[13] T. R. Whitehead, T. Poxon-Pearson, F. M. Nunes, and G. Potel, Phys. Rev. C **105**, 054611 (2022).

[14] Y. Litvinov, S. Bishop, K. Blaum, F. Bosch, C. Brandau, L. Chen, I. Dillmann, P. Egelhof, H. Geissel, R. Grisenti *et al.*, Nucl. Instrum. Methods Phys. Res., Sect. B **317**, 603 (2013).

[15] M. Steck and Y. A. Litvinov, Prog. Part. Nucl. Phys. **115**, 103811 (2020).

[16] H. Geissel, P. Armbruster, K. Behr, A. Brünle, K. Burkard, M. Chen, H. Folger, B. Franczak, H. Keller, O. Klepper *et al.*, Nucl. Instrum. Methods Phys. Res., Sect. B **70**, 286 (1992).

[17] J. Glorius, Y. A. Litvinov, M. Aliotta, F. Amjad, B. Brückner, C. Bruno, R. Chen, T. Davinson, S. Dellmann, T. Dickel *et al.*, Nucl. Instrum. Methods Phys. Res., Sect. B **541**, 190 (2023).

[18] M. Kühnel, N. Petridis, D. Winters, U. Popp, R. Dörner, T. Stöhlker, and R. Grisenti, Nucl. Instrum. Methods Phys. Res., Sect. A **602**, 311 (2009).

[19] J. Eichler and T. Stöhlker, Phys. Rep. **439**, 1 (2007).

[20] Micron Semiconductor LTD, http://www.micronsemiconductor.co.uk/.

[21] E. Rutherford, London, Edinburgh, Dublin Philos. Mag. J. Sci. **21**, 669 (1911).

[22] Y. Xing, J. Glorius, L. Varga, L. Bott, C. Brandau, B. Brückner, R. Chen, X. Chen, S. Dababneh, T. Davinson *et al.*, Nucl. Instrum. Methods Phys. Res., Sect. A **982**, 164367 (2020).

[23] See Supplemental Material at http://link.aps.org/supplemental/10.1103/PhysRevLett.134.082701 for values of intermediate analysis steps for cross sections of ^{124}Xe(p, γ) and ^{124}Xe(p, n).

[24] N. Iwasa, H. Weick, and H. Geissel, Nucl. Instrum. Methods Phys. Res., Sect. B **269**, 752 (2011).

[25] M. Steck, P. Beller, K. Beckert, B. Franzke, and F. Nolden, Nucl. Instrum. Methods Phys. Res., Sect. A **532**, 357 (2004).

[26] A. N. Artemyev, A. Surzhykov, S. Fritzsche, B. Najjari, and A. B. Voitkiv, Phys. Rev. A **82**, 022716 (2010).

[27] B. Fischer, Nucl. Instrum. Methods Phys. Res., Sect. B **30**, 284 (1988).

[28] A. J. Koning, S. Hilaire, and M. C. Duijvestijn, AIP Conf. Proc. **769**, 1154 (2005).

[29] T. Rauscher, Astrophys. J. Suppl. Ser. **201**, 26 (2012).

[30] E. Bauge, J. P. Delaroche, and M. Girod, Phys. Rev. C **63** (2001).

[31] S. Goriely, N. Chamel, and J. M. Pearson, Phys. Rev. C **88**, 024308 (2013).

[32] S. Goriely, S. Hilaire, and A. J. Koning, Phys. Rev. C **78**, 064307 (2008).

[33] S. Goriely, S. Hilaire, S. Péru, and K. Sieja, Phys. Rev. C **98**, 014327 (2018).

[34] A. Koning, S. Hilaire, and S. Goriely, Nucl. Phys. **A810**, 13 (2008).

[35] V. Plujko, O. Gorbachenko, R. Capote, and P. Dimitriou, At. Data Nucl. Data Tables **123–124**, 1 (2018).

[36] S. Goriely and V. Plujko, Phys. Rev. C **99**, 014303 (2019).

[37] P. Möller, A. Sierk, T. Ichikawa, and H. Sagawa, At. Data Nucl. Data Tables **109–110**, 1 (2016).